ionization of delocalized molecular orbitals yields *delocalized* hole states. According to a theoretical model of Snyder,[40] delocalization of a hole over t centers gives a relaxation energy per center of approximately $1/t^2$ that for a localized hole. Hence one would not expect the relaxation energies to be similar. The data appear to support the proposition that the ionization of delocalized lone pairs made up of weakly interacting atomic orbitals yields localized hole states. Indeed, in recent years, other investigators have made similar proposals regarding excited and ionized valence shells.[42-46] It appears that, just as in the case of mixed-valence compounds, the lifetime of the localized state (or the rate of electron transfer from one site to another) is the relevant factor to be considered when deciding whether a hole is localized or delocalized.

The two exceptional molecules, CF_4 and OF_2, contain fluorine atoms attached to small, first-row atoms and are examples of molecules in which the fluorine atomic orbitals making up the lone-pair orbitals interact significantly. Ascribing antibonding character to these lone-pair orbitals is probably equivalent to saying that the ionized states are delocalized instead of localized. Related evidence for delocalization effects have been observed in the Auger spectra of tetrahedral halides.[47]

Concluding Remarks

Clearly the LOIP concept, involving both core and valence ionization potentials, is a valuable aid in the assignment of valence-shell photoelectron spectra. It also provides grist for the mill of theoreticians, for example, with respect to the question of the localized or delocalized character of valence holes. However, its main value is in providing chemists with a reliable method for interpreting valence-shell ionization potentials in terms of the bonding or antibonding character of molecular orbitals. Typical applications are the determination of the degree of interaction of so-called lone-pair orbitals (mainly comprised of p or d orbitals) either with filled orbitals (bonding orbitals or other lone pairs) or with empty orbitals (antibonding orbitals or higher energy d orbitals). It is significant that the LOIP method allows chemists to make these interpretations using only experimental data, free from most of the calculational difficulties and interpretative ambiguities of theoretical methods.

It is a pleasure to acknowledge the contributions of my students and colleagues who are listed as coauthors in the cited references. I am indebted to Professors T. D. Thomas of Oregon State University and D. L. Lichtenberger of the University of Arizona for their encouragement. This work was supported by the Director, Office of Energy Research, Office of Basic Energy Sciences, Chemical Sciences Division of the U.S. Department of Energy under Contract No. DE-AC03-76SF00098.

(41) Bagus, P. S.; Schaefer, H. F. *J. Chem. Phys.* **1972**, *56*, 224.
(42) Sawatzky, G. A.; Lenselink, A. *J. Chem. Phys.* **1980**, *72*, 3748.
(43) Benard, M. *Chem. Phys. Lett.* **1983**, *96*, 183.
(44) Keijzers, C. P.; Bagus, P. S. *J. Chem. Phys.* **1978**, *69*, 4032.
(45) Muller, J.; Poulain, E.; Goscinski, O.; Karlson, L. *J. Chem. Phys.* **1980**, *72*, 2587.
(46) Jonkers, G.; De Lange, C. A.; Noodleman, L.; Baerends, E. J. *Mol. Phys.* **1982**, *46*, 609 and references therein.
(47) Rye, R. R.; Houston, J. E. *J. Chem. Phys.* **1983**, *78*, 4321.

Nonlinear Optical Spectroscopy of Molecular Systems†

R. M. HOCHSTRASSER* and H. P. TROMMSDORFF

Department of Chemistry, University of Pennsylvania, Philadelphia, Pennsylvania 19104, and Laboratoire de Spectrométrie Physique associé au CNRS, Université Scientifique & Médicale de Grenoble, BP68, 38402, St. Martin d'Hères, France

Received October 18, 1982 (Revised Manuscript Received April 18, 1983)

The study and application of nonlinear optical spectroscopy in chemical problems was made possible by the development of tunable lasers. The giant flashlamps of the prelaser era produced optical power at a given wavelength of at most 10^{-4} of the power of even the simplest narrow-band tunable laser. Nonlinear optical processes depend on the square or cube of the optical power so that the minimum enhancement factor for lasers over conventional sources is 10^8–10^{12}! Conventional picosecond laser pulses can have peak powers of 20 GW, superior to the total capability of a major hydroelectric scheme or nuclear power plant. Clearly these devices do not simply extend the properties of the older light sources: they open doors to the study of totally new concepts in the interaction of molecules with light.

When molecules are placed in intense optical fields, a variety of effects occur. The molecule may fragment, rearrange, or undergo ionization. On the otherhand, the ensemble of molecules can bring about the creation of new optical fields in so-called coherent processes. The frequency and time dependence of these new fields carry hitherto unknown information about the molecular states and their dynamics. Studies of such non-

Robin M. Hochstrasser is the Blanchard Professor of Chemistry and Director of the Regional Laser Laboratories at the University of Pennsylvania. He was born and educated in Scotland receiving his Ph.D. from Edinburgh University in 1955. He migrated to Canada in 1957 and to the U.S. and the University of Pennsylvania in 1963. His research is concerned with laser studies of molecular relaxation processes and spectroscopy, particularly of large molecules, molecular crystals and proteins.

H. Peter Trommsdorff was born in Darmstadt, Germany, and educated in Austria and Germany. He studied physics at the University of Göttingen and received his Doctorat d'Etat in 1972 from the University of Grenoble. His research interests concern molecular excited states and dynamics in condensed phases. He has been involved in collaborative research efforts with the group at the University of Pennsylvania since 1973.

†This research was supported by grants from NIH (GM12592), the Army Research Office (AROD DAAG-29-80-C-0014), the National Science Foundation CHE8303916, and in part by NSF/MRL DMR-7923647. R.M.H. and H.P.T. acknowledge support from the U.S.–France (NSF–CNRS) program through grant INT-8213024.

0001-4842/83/0116-0376$01.50/0

linear interactions are of great value in molecular spectroscopy, chemical kinetics, chemical analysis, in the study of fundamental processes such as ionization, energy transfer, and internal energy reorganization, and in the study of dynamics in liquids and solids. Some applications of various types of nonlinear spectroscopy are described in this Account, which attempts also to provide a framework upon which to understand the nature of the nonlinear processes themselves.

Conventional optical absorption spectroscopy involves measurements of the frequency or wavelength dependence of the changes brought about in the intensity of light in passing it through a sample: the absorption coefficients are not dependent on the intensity of the incident beam. One way to think about ordinary spectroscopy is that the incident-light electric field $E(t)$ at a particular frequency ω induces dipole moments in the molecules, which sum up to form a macroscopic polarization P, according to

$$P(t) = \chi(\omega)E(t) \tag{1}$$

In effect the medium supports the driving field in the form of an oscillating dipole moment. Equation 1 is the macroscopic form of the well-known relation $\mu = \alpha E$ between the induced dipole moment and the applied field, with α being the polarizability. The amount of light that is transmitted at frequency ω is determined by the amplitude of the polarization wave at the exit window of the absorption cell. Absorption occurs because the polarization wave is diminished by coupling the light to the medium. This is most efficient when the natural frequencies of the medium, or molecular transitions, match the incident-light frequency. Under these circumstances relaxation properties of the medium, such as fluorescence or changes in energy brought about by collisions, will effectively cause the macroscopic polarization to be diminished as energy is transferred from the field into other modes.

When the light comes from a laser, the macroscopic polarization wave amplitude is no longer obtained accurately from eq 1 but instead is of the form

$$P(t) = \sum_n \chi^{(n)}(\omega,\omega', \ldots)E^n(t) \tag{2}$$

This polarization can have many different frequency components. For example, if $E(t) = E \cos \omega t$, then $E^3(t) = (E^3/4)(3 \cos \omega t + \cos 3\omega t)$, so that $P(t)$ oscillates at ω *and* 3ω. Even more frequency components arise when $E(t)$ itself consists of more than one frequency, such as occurs in many nonlinear experiments. For example, for $E(t)$ consisting of fields at ω_1 and ω_2 it is easy to show that, for $n = 3$, $P(t)$ has components oscillating at ω_1, $3\omega_1$, ω_2, $3\omega_2$, $2\omega_1 + \omega_2$, $2\omega_2 + \omega_1$, $2\omega_1 - \omega_2$, and $2\omega_2 - \omega_1$. Each of these so-called Fourier components that has amplitude at the exit window of the cell produces light at the specified frequency. The generated radiation travels in a well-defined direction, just as in the linear absorption experiment. The amplitude of each wave is determined by the resonance between these frequencies and the transitions of the medium and by the dynamical processes that diminish or damp the macroscopic polarizations induced by the driving fields. The nonlinear polarizabilities of the medium, $\chi^{(n)}$, are termed nonlinear susceptibilities, and a detailed treatment[1-4] shows that each generated wave is governed by a particular susceptibility, corresponding to a particular manner of response of the medium to the set of frequencies involved. Thus, nonlinear spectroscopy, which is the study of these generated waves for $n \geq 2$, can yield considerably more information about the molecular structure and dynamics than could be obtained from studying the linear response of a system to a single frequency.

Coherence Loss

Whenever the Fourier components of the applied fields are resonant with a molecular level pair i, j, the polarization wave is damped at a rate Γ_{ij}: $1/\Gamma_{ij}$ is called the T_2 time for the specified level pair. Within certain statistical approximations that are expected to be valid in homogeneous condensed phases, the rate of coherence loss is given by

$$\Gamma_{ij} = 1/T_2 = \tfrac{1}{2}(\gamma_i + \gamma_j) + \Gamma_{ij}' \tag{3}$$

where the first term is the average of the population decay rates of the two levels and Γ_{ij}' is the so-called "pure" dephasing rate—a term that results in damping of the coherent polarization without loss of population in the levels i and j. Line-width measurements yield only Γ_{ij}; population decay measurements yield γ_i and γ_j. Normally Γ_{ij}' is obtained by difference, but as we shall see there are ways to measure it directly by nonlinear methods. The light intensity emitted in the directional beam is proportional to the square of the appropriate component of its polarization so that we expect it to depend inversely on Γ_{ij}^2 in the steady state. Experiments in the frequency domain are usually carried out in a steady-state condition in which the pulse duration of the driving fields are long compared with the time scales $1/\Gamma_{ij}$ for decay of the coherence.

The Molecule-Field Interaction

Our research concerns mainly $\chi^{(3)}$, the lowest order nonlinear susceptibility that has nonzero components in all media. In its role as a function describing the response of the system to a particular set of fields, $\chi^{(3)}$ contains all the microscopic information regarding the transition moments, resonance energy denominators, anisotropy, as well as the polarization and population decay parameters.

The calculation of the susceptibility from quantum statistical mechanics predicts that the time ordering of the interacting fields is an important factor in a nonlinear process. For example, in a third-order process involving three fields interacting with the medium to produce a new wave, one can conceive of eight different time orderings for the ingoing fields. These arise in the following way. Each real field $E_i(t)$ can be written in the form $E_i(t) = \epsilon_i e^{-i\omega_i t} + \epsilon_i^* e^{-i\omega_i t}$, so that in the product of three fields we find terms of the type $\epsilon_i\epsilon_j^*\epsilon_k e^{-i(\omega_i-\omega_j+\omega_k)t}$ and so on. We see that the different generated fields correspond to different combinations of the complex components of the ingoing waves. Knowing this we can drop explicit mention of the time dependence in the outgoing wave, since it is obvious that a frequency $(\omega_i - \omega_j + \omega_k)$ must derive from the field product $\epsilon_i\epsilon_j^*\epsilon_k$.

(1) N. Bloembergen, "Nonlinear Optics", Benjamin, New York, 1965.
(2) P. N. Butcher, "Nonlinear Optical Phenomena", Engineering Experiment Station, Ohio State University, Columbus, OH, 1965.
(3) R. W. Hellwarth, *Prog. Quantum Electron.*, **5**, 1 (1977).
(4) D. C. Hanna, M. A. Yuratich, and D. Cotter, "Nonlinear Optics of Free Atoms and Molecules", Springer Series in Optical Sciences, Springer-Verlag, New York, 1979.

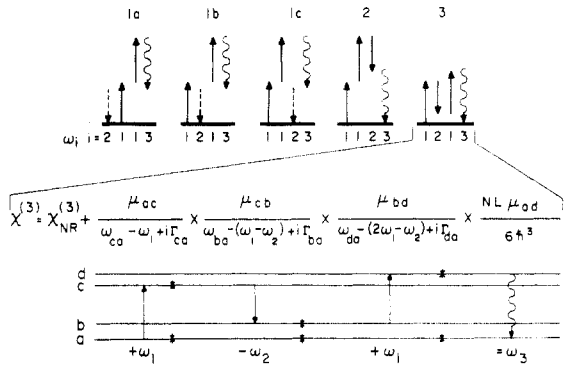

Figure 1. Diagrams representing various third-order processes resulting from two incident-light fields, ω_1 and ω_2, generating a new wave at $\omega_3 = 2\omega_1 - \omega_2$. The lower portion shows the evolution of the explicit susceptibility shown in the case diagram 3 occurs with ω_1, $\omega_1 - \omega_2$, and ω_3 matching molecular transition frequencies.

There are, however, six different ways to time order the effect of these three fields on the medium, and each of these represents a separate process adding its own contribution to the total susceptibility. Often the time ordering is represented by the ordering of the frequency arguments, as in $\chi^{(3)}(\omega_i, -\omega_j, \omega_k)$, which implies first interact the system with ϵ_k and then with ϵ_j* and finally with ϵ_i. Of course in many experiments all the fields are present simultaneously, but it is often the case that some particular sequence dominates a particular signal. The number of time-ordered contributions can be large so it is helpful to use simple diagrams to represent them.

Figure 1 shows diagrams representing some of these time orderings in which we have chosen $\omega_1 > \omega_2$ so that $2\omega_1 - \omega_2$ is a larger frequency than either ω_1 or ω_2. The solid and dashed arrows refer to changes in the wave function or its complex conjugate. A transition dipole μ_{ab} is the probability amplitude for a photon to be created as the wave function changes according to $\psi_b \rightarrow \psi_a$*, whereas μ_{ab}* = μ_{ba} implies a photon is annihilated as the wave function transforms in the manner $\psi_a \rightarrow \psi_b$*. The process of "absorption" of light goes as $|\mu_{ab}|^2$ and could be represented diagramatically as two energy levels connected by up and down solid arrows or down and then up dashed arrows. This is because $|\mu_{ab}|^2 = \mu_{ab}\mu_{ba} = \mu_{ab}$*$\mu_{ba}$*. Thus, the time ordering in the diagrams has t increasing from left to right with the solid and dashed arrows corresponding to transition moments and their complex conjugates or time-reversed forms. These arrows represent *amplitudes*; the coherent light emission involves the square of the terms represented by these diagrams. Figure 1 illustrates how simple diagrams can be used to represent the steps involved in each of the various time orderings, and inspection of the diagrams readily yields the conditions for resonant enhancement. The diagrams reflect the steps leading to particular terms in the third-order response that are *resonant*. The first transition must involve a previously populated state, and it creates a coherence between the initial and final states of the transition. In subsequent steps the transition arrows are added as vectors, and coherence is created in the pair of states coupled by the vector resultant. The resultant of three waves equals the outgoing, or fourth wave, represented in the diagrams as a wavy line connecting the two states whose coherence is responsible for the macroscopic polarization. For example, the process described by diagram 1 consists of three distinct diagrams 1a–1c that involve the same response of molecules to the fields, whereas in Figures 1.2 and 1.3 only one time ordering can be involved. The lower portion of Figure 1 shows the effect on diagram 3 of introducing molecular energy levels at combinations of the laser frequencies. The form of third-order susceptibility that would arise from each resonant step is also given. The asterisks mark the level pairs into which coherence is introduced by the relevant-light field in each step.[5] Each damping parameter is associated with a particular level pair. The fully resonant system is thus seen to arise from the presence of four levels including the initial state, and it is triply resonant (i.e., it has three energy denominators that can become as small as is the appropriate Γ when the resonance condition is achieved). In general, all five of the diagrams shown in Figure 1 would contribute to a coherent signal at $2\omega_1 - \omega_2$, the common feature being that two photons are removed from the ω_1 beam while a photon at ω_3 is generated. However 1, 2, or 3 might dominate the signal if the molecule were to have allowed transitions in the appropriate regions. There are many other diagrams that contribute to the generation of light at $2\omega_1 - \omega_2$ besides those shown in Figure 1.

Single-Resonance Responses

Singly resonant contributions to the susceptibilities are those for which only one resonance condition is nearly fulfilled. These resonant contributions occur when the difference or the sum of the frequencies of two incident fields equals the energy difference of a pair of levels connected by a Raman or a two-photon absorption process or when either ω_1 or ω_2 or the outgoing wave ω_3 resonates in a one-photon process. At least one of the two levels involved in the resonance must be populated in order to observe such resonances. A system may have any number of singly resonant contributions and the susceptibility has the form:

$$\chi = \left\langle \chi_{NR} + \sum_{b,l} \frac{A_{ba}}{\omega_{ba} \pm i\Gamma_{ba} - \{\omega_l\}} \right\rangle \qquad (4)$$

$\{\omega_l\}$ stands for each of the combinations of the frequencies of the incident fields satisfying $\omega_{ba} \approx \{\omega_l\}$, the sign of $i\Gamma$ is determined by the specific resonant process, and the angle brackets indicate that such singly resonant contributions are to be summed over all species present in a unit volume of the sample. The species may be different molecules or the same molecules in different environments or states.

χ_{NR} is often a real quantity giving the contribution of all nonresonant transitions for which the frequency mismatch is much larger than the damping parameter. The coherently generated light intensity is proportional to $|\chi^{(3)}|^2$ and so it consists of the sum of the squares of the real and imaginary parts of eq 4. The variation with frequency of a susceptibility of this type thus leads to the determination of resonance frequencies ω_{ba}, the

(5) When light of frequency ω interacts with a molecule in state ψ_a, if there is another state ψ_b for which μ_{ab} exists, and the photon energy $\hbar\omega$ is approximately equal to $E_b - E_a$, then the system is driven into a state that is a superposition of ψ_a and ψ_b by the light. The *coherence* in the *ensemble* is a measure of how similar are these superpositions in the different molecules. When all superpositions are identical, the macroscopic polarization is maximum, and in the other extreme, when they are randomly phased, the polarization is lost—the coherence has decayed.

corresponding damping parameter Γ_{ba}, and the amplitude of the resonance measured with respect to the nonresonant background A_{ba}/χ_{NR}.

Single Resonances at $\omega_1 - \omega_2$ and $2\omega_1$

Most experimental studies of singly resonant terms have concerned Raman and two-photon resonances using $\chi^{(3)}$, the lowest order susceptibility to which these resonances contribute.[6-9] Four-wave mixing arising from two different input frequencies ω_1, ω_2 and monitored by the intensity of light generated by the induced polarization at $\omega_3 = 2\omega_1 - \omega_2$ has emerged as a versatile method of measuring singly resonant $\chi^{(3)}$ in gases, liquids, and solids. The frequencies of all light beams involved in this situation are similar, and phase matching (see below) is therefore easy to achieve in all media, yet the directional signal at $2\omega_1 - \omega_2$ is readily isolated. The generated beam can be chosen so that $\omega_3 > \omega_1 > \omega_2$ or that $\omega_3 < \omega_1 < \omega_2$. These Raman resonant contributions were given the acronyms CARS and CSRS, for Coherent AntiStokes (or Stokes) Raman Scattering/Spectroscopy. When $\chi_{NR}^{(3)}$ is real, both methods lead to the same spectral shapes for a given resonant level pair though only CARS uses the plus sign in eq 4.

In conventional spontaneous Raman spectroscopy the spectral resolution is about 0.2 cm^{-1}. Improvements can be accomplished by means of expensive interferometric methods. In contrast, the spectral resolution in CARS is determined by the spectral bandwidth of the lasers. It was therefore natural to use CARS for high-resolution gas-phase Raman spectroscopy and to probe the chemical composition and temperature distribution within flames.[10] The generation of light at the anti-Stokes frequency is resonance enhanced when $\omega_1 - \omega_2$ matches a transition frequency and also when there are two-photon resonances. The polarization in a medium displaying both Raman and two-photon effects takes the form

$$P^{(3)} = \left\langle \chi_{NR} + \frac{A_{ba}}{\omega_{ba} - (\omega_1 - \omega_2) + i\Gamma_{ba}} + \frac{T_{ca}}{\omega_{ca} - 2\omega_1 + i\Gamma_{ca}} \right\rangle \quad (5)$$

where ω_{ca} marks the energy of an electronic state c above the ground state a. T_{ca} is a constant that vanishes unless the two-photon selection rules are obeyed for the transition a → c. A_{ba} can be related to the Raman cross section. The comparatively low probability of two-photon absorption processes has resulted in the development of many indirect detection methods, but it is often not practical to use such techniques to determine absolute cross sections. Coherent signals are more readily calibrated.

We used a coherent method for this purpose in our studies of the two-photon spectra of NO.[11] The quantitative calibration of these four wave mixing measurements in which a → c corresponded to the $\chi^2 \rightarrow a^2\Sigma$ transition of NO was achieved by measuring under identical beam conditions the ω_{ba} = 2331 cm^{-1} Raman (CARS) resonance of N_2 in air, for which the Raman scattering cross section is known. In these early measurements the laser line widths were larger than the spectral widths of the transitions. State-of-the-art approaches avoid such problems by using transform limited pulses obtained by amplifying single mode tunable dye laser beams to the appropriate power levels. In the case of NO, energy levels corresponding to transition energies of about 44 000 cm^{-1} were studied with use of visible light (see Figure 2). In this case the signal at $2\omega_1 - \omega_2$ is enhanced for each rovibronic transition a → c satisfying $\omega_{ca} = 2\omega_1$. The observed spectrum matches one obtained earlier[12] by two-photon fluorescence excitation.

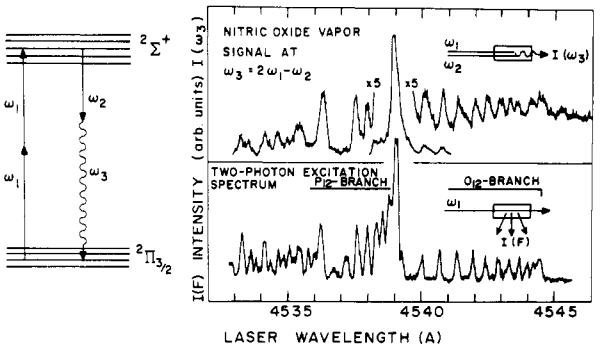

Figure 2. Comparison of the two-photon resonance in NO observed by four-wave mixing (a) and two-photon excitation experiments (b). In spectrum a the intensity at $\omega_3 = 2\omega_1 - \omega_2$ is plotted against the wavelength of the ω_1 beam; ω_2 being constant. In the spectrum b the intensity of fluorescence resulting from two-photon absorption is given as a function of the excitation wavelength.

So far we have not considered the optics of these nonlinear processes. In the case where there are incident fields E each having two counterrotating parts: e.g., $E = \epsilon e^{-i\omega t} + \epsilon^* e^{i\omega t}$, then $\epsilon = |\epsilon| e^{i\mathbf{k}\cdot\mathbf{r}}$ where $\mathbf{k}$ is the propagation wavevector of the light. In transparent media it is found that $|\mathbf{k}| = n\omega/c$. The signal generated from any combination of positive or negative frequency components of the incident fields is maximized when the generated light wavevector $\mathbf{k}_s$ equals the sum of the individual field component wavevectors. For example, the signal at $2\omega_1 - \omega_2$ that is brought about through a term involving $\epsilon_1\epsilon_2^*\epsilon_1$ is optimized when $\mathbf{k}_s = 2\,\mathbf{k}_1 - \mathbf{k}_2$. The signals are always generated in the directions $2\mathbf{k}_1 - \mathbf{k}_2$ by virtue of momentum conservation for photons, but $\mathbf{k}_s = 2\mathbf{k}_1 - \mathbf{k}_2$ defines the optimum choice and is known as the phase-matching condition.

Single Resonances in Molecular Crystals

Studies in anisotropic crystals are experimentally more demanding but yield information about the molecular anisotropy and allow the evaluation of individual tensor elements.[13] The amplitudes of the two-photon or Raman resonance signals are simple related to the cross sections for the corresponding incoherent pro-

(6) R. D. Maker and R. W. Terhune, *Phys. Rev. A*, **137**, 801 (1965).
(7) M. D. Levenson, C. Flytzanis, and N. Bloembergen, *Phys. Rev. B*, **6**, 3962 (1972).
(8) S. D. Kramer, F. G. Parson, and N. Bloembergen, *Phys. Rev. B*, **9**, 1853 (1974); S. D. Kramer and N. Bloembergen, *ibid.*, **14**, 4654 (1976).
(9) M. D. Levenson and N. Bloembergen, *Phys. Rev. B*, **10**, 4447 (1974); *J. Chem. Phys.*, **60**, 1323 (1974).
(10) P. Regnier and J.-P.E. Taran, *Appl. Phys. Lett.*, **23**, 240 (1973); P. Regnier, F. Moya, and J.-P.E. Taran, *AIAA3*, **12**, 826 (1974); F. Moya, S. A. J. Druet, and J.-P.E. Taran, *Opt. Commun.*, **13**, 169 (1975).
(11) R. M. Hochstrasser, G. R. Meredith, and H. P. Trommsdorff, *Chem. Phys. Lett.*, **53**, 423 (1978).
(12) R. G. Bray, R. M. Hochstrasser, and J. E. Wessel, *Chem. Phys. Lett.*, **27**, 167 (1974).
(13) R. M. Hochstrasser, G. R. Meredith, and H. P. Trommsdorff, *J. Chem. Phys.*, **73**, 1009 (1980).

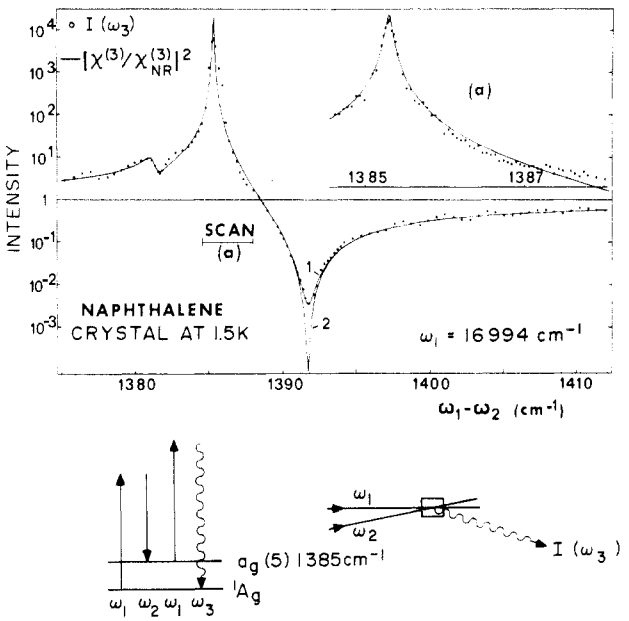

Figure 3. Four-wave mixing spectra of a naphthalene crystal. The intensity of the beam at $\omega_3 = 2\omega_1 - \omega_2$ (dots) was measured as ω_2 was scanned. The continuous trace represents $|\chi^{(3)}/\chi_{NR}^{(3)}|^2$ calculated from a dispersion formula like eq 5 but including two single Raman resonances of 1381.2 and 1385.3 cm^{-1}. After ref 14.

cesses of two-photon absorption and Raman scattering. In the gas phase these are obtained from the orientationally averaged molecular tensor elements. In the condensed phase the molecules experience the intensity of the light field within the dielectric. Hence, local field factors have to be included when relating the molecular tensor element to the resonance amplitude. With use of Raman cross sections for the calibration, accurate measurements of $\chi_{NR}^{(3)}$ and two-photon tensors of individual vibronic transitions have been made in several simple organic crystals at low temperature. The coherent signal in these experiments can easily be measured over an extremely large dynamic range and line shapes can be accurately determined with narrow-band lasers. Figure 3 shows the CARS spectrum of a pure naphthalene crystal.[14] In this case the stronger Raman resonance could be fitted to a single Lorentzian line with a Γ of 0.03 cm^{-1} corresponding to an excited state lifetime of 90 ps.

A fundamental problem in the analysis of line shapes in the condensed phase is the evaluation of inhomogeneous contributions. In the case of the pure crystal of naphthalene these are considered to be reduced to a negligible level as a result of the delocalization of the 1385-cm^{-1} excitation: the inhomogeneous frequency distribution is not sensed by the delocalized excitons. Dynamics of vibrational state relaxation in crystals can be confirmed in time domain experiments in which ω_1 and ω_2 first creat the coherence between the $V = 0$ and $V = 1$ levels, and this coherence is probed at a later time by an ω_1 beam. A measurement of the decay of the light field generated at frequency $\omega_3 = 2\omega_1 - \omega_2$ yields the coherence decay parameter, Γ, for the two-level system. If in time domain experiments the light *intensity* is measured, the observed decay constant is expected to be 2Γ. In the case of the naphthalene crystal 1385-cm^{-1} band, time domain experiments yielded an exponential

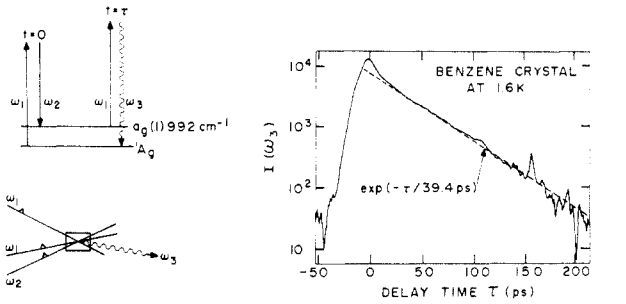

Figure 4. CARS signal from a benzene crystal at 1.6 K as a function of the delay time of the second ω_1 beam with respect to the time synchronized ω_2 and first ω_1 beams (ω_1 = 18170 cm^{-1}, $\omega_1 - \omega_2$ = 991 cm^{-1}). All fields are polarized parallel to a crystal axis. The picosecond pulses were produced by two dye lasers synchronous by pumped by a mode-locked Ar$^+$ laser. After ref 16.

decay constant in excellent agreement with the CARS value.[15]

The benzene crystal presents a simpler example. The 991-cm^{-1} ring-stretching mode forms an exciton band in the crystal that can be excited to its lowest energy Davydov component by proper choice of the polarization of the incident beams. Figure 4 shows a measurement of the coherence decay by picasecond time-resolved CARS for this mode.[16] The decay is a single exponential over three decades and the decay time measured (39 ± 2 ps) is in full agreement with frequency domain measurements (39 ± 2 ps) carried out in this laboratory.[17]

Similar measurements on solid N_2 at 2 K did not show such a simple decay of the coherence.[18] Population decay of the $V = 1$ to $V = 0$ state in N_2 takes seconds and does not contribute to the signals observed on the nanosecond time scale. The nonexponential decay for N_2 was explained in terms of incoherent scattering of the 2328-cm^{-1} vibron on statistically distributed crystal defects, the effective decay ranging from less than 1 ns at short times to ~15 ns at longer delay times (100 ns). These experiments probe the time development of the exciton-like waves introduced into the materials by light. Both elastic and inelastic effects contribute to the diminution of the wave amplitudes (loss of coherence). One elastic effect arises from disorder that causes the wave to be scattered into other wavelets having the same total energy. Spontaneous decay, such as vibrational relaxation, is an example of an inelastic process. In the case of the N_2 crystal the decay is entirely due to elastic processes, whereas in the aromatic molecular crystals the coherence is diminished by vibrational decay processes as well.

A variety of experiments on organic solids have now been accomplished by using such techniques so that a substantial pool of information on vibrational relaxation times in these systems is now available. The fundamental modes of aromatics invariably show vibrational relaxation in the range of 5–10^3 ps. For example, the 854-cm^{-1} (e_{1g}) mode of benzene has a relaxation time of 450 ps.[17] These times are sufficiently long to be

(14) P. L. DeCola, R. M. Hochstrasser, and H. P. Trommsdorff, *Chem. Phys. Lett.*, **72**, 1 (1980).

(15) B. H. Hesp and D. A. Wiersma, *Chem. Phys. Lett.*, **75**, 423 (1980).

(16) F. Ho. W.-S. Tsay, J. Trout, and R. M. Hochstrasser, *Chem. Phys. Lett.*, **83**, 5 (1981).

(17) R. Bozio, P. L. DeCola, and R. M. Hochstrasser, submitted for publication.

(18) I. I. Abram, R. M. Hochstrasser, J. E. Kohl, M. G. Semack, and D. White, *J. Chem. Phys.*, **71**, 153 (1979).

studied by conventional picosecond methods. It remains as a problem for the future to identify the key properties of the intermolecular potential responsible for these relaxation processes and the resulting pathways toward thermal equilibrium.

Resonances at ω_1 and ω_2

In the foregoing examples the single resonance condition was met by having either $2\omega_1$ or $\omega_1 - \omega_2$ match a molecular transition frequency. Resonances with ω_1 and/or ω_2 are also very useful for spectroscopic and dynamical studies. Two such examples that we have used to study liquid-state processes are polarization spectroscopy and coherent Rayleigh mixing. In polarization spectroscopy, first discussed in relation to gases,[19] the sample is pumped with light at ω_1 and the induced birefringence is probed with a beam at ω_2. When ω_2 is scanned, a resonance is expected when $\omega_1 - \omega_2$ matches a molecular transition. Such resonances were recently studied also for porphyrins in liquids[20] and they suggest a promising approach to understanding the nature of solution spectra of complex molecules.

An important question regarding the structure of solutions is whether or not they are homogeneous on the time scale of the response of the system to light. It is not hard to imagine why a solution might be inhomogeneous as a result of solute molecules being, at any instant, in a wide range of environments and spanning a wide range of internal energies. In the former case the inhomogenieties might be expected to persist over the time scale of the diffusional and rotational correlations, but in the latter a wide range of vibrational relaxation processes serve to homogenize the system. On the other hand, the coherent response to the driving fields is damped at least as rapidly as the phase interrupting collision frequency in the liquid. The question therefore reduces to whether Γ_{ij} is larger than the homogenization rates. It appears that certain solutions at normal temperatures are inhomogeneous on time scales that are long compared with the collision frequencies. These issues can be confronted by a number of nonlinear optical methods, one of which is coherent Rayleigh mixing.

In coherent Rayleigh mixing experiments the incident and the generated frequencies are chosen to be nearly equal in order that the frequency difference $|\omega_1 - \omega_2|$ be comparable with the rates of the various relaxation processes occurring in the sample. The dynamics of the states involved in the optical transition are explored by measuring the intensity of the generated beam at $2\omega_1 - \omega_2$ as a function of the frequency difference $|\omega_1 - \omega_2|$. The way in which these experiments probe the dynamics can be envisioned by considering the spatial distribution of light intensity set up in the sample by two intersecting incident beams: for two beams of equal frequency ω and field strength E crossing in the sample at an angle of 2θ, the intensity in the sample is spatially periodic:

$$|E_1 + E_1'|^2 = 4E^2 \cos^2 [2\pi y \sin \theta/\lambda] \qquad (6)$$

corresponding to a stationary diffraction grating along the direction y that is parallel to $\vec{k}_1 - \vec{k}_1'$. Another beam ω_2 will diffract from this grating with the overall process

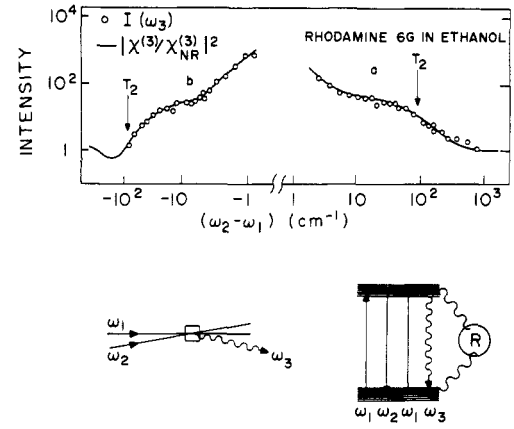

Figure 5. Rayleigh type mixing spectrum of rhodamine 6G in ethanol: note that the frequency scale is logarithmic. The continuous line represents the best theoretical fit based on the response of a two-level system plus a reservoir to the two driving fields. The "steps" at a and b occur because of the inhomogeneous broadening in the model. After ref 21.

leading to the generation of a beam at ω_2 in the direction $\mathbf{k}_1 - \mathbf{k}_1' + \mathbf{k}_2$. It is easy to see that this corresponds to the Bragg diffraction condition for a grating having the character of eq 6. When the frequencies of the two beams creating the grating differ by an amount $\Delta\omega = \omega_1 - \omega_2$, the spatial intensity distribution is no longer stationary and the diffracted beam will be Doppler shifted by an amount $\Delta\omega$: The diffraction of ω_1 gives rise to light emitted at frequency $2\omega_1 - \omega_2$. The amplitude of the grating and therefore the intensity of the diffracted beam is determined by the variation of the refractive index of the medium that is induced by the incident E_1 fields. Different contributions to this variation stem from thermal, population, and coherence transfer processes, and these contributions build up and decay with different characteristic time constants. In a moving grating, therefore, only contributions with characteristic time constants faster than $1/\Delta\omega$ will show up, otherwise they will be washed out, and this is how the dynamics of the medium can be probed by varying the frequency difference of the two beams creating the grating. For example, with incident visible beams separated by 0.1 nm, processes occurring on the time scale of 5 ps are singled out.

The results of such experiments require to be fitted to models of the molecular response and therefore they measure parameters of the model. Thus an important part of research of this type is the generation and systematic testing of these models. A dye with a large fluorescence quantum yield when pumped with ω_1 into the region of its vibrationless excited electronic state corresponds approximately to the model of an inhomogeneous distribution of three-level systems. The three levels correspond to the ground state, first excited state, and a reservoir that can absorb energy but not interact with the light.[21] The Rayleigh mixing results in Figure 5 were obtained with rhodamine 6G (Rh-6G) irradiated with two beams having nearly equal frequency ($\omega_1 \approx \omega_2$) in the range of the first electronic transition. A qualitive change in the intensity of the generated beam is expected when $\omega_1 - \omega_2 \approx \Gamma$ even when the actual linear absorption spectrum is much larger than Γ due to inhomogeneous broadening. In fact, the

(19) C. Wieman and Th. W. Hänsch, *Phys. Rev. Lett.*, **36**, 1170 (1976).
(20) J. R. Andrews and R. M. Hochstrasser, *Proc. Natl. Acad. Sci. U.S.A.*, **79**, 3110 (1980).
(21) H. Souma, E. J. Heilweil, and R. M. Hochstrasser, *J. Chem. Phys.*, **76**, 5693 (1982).

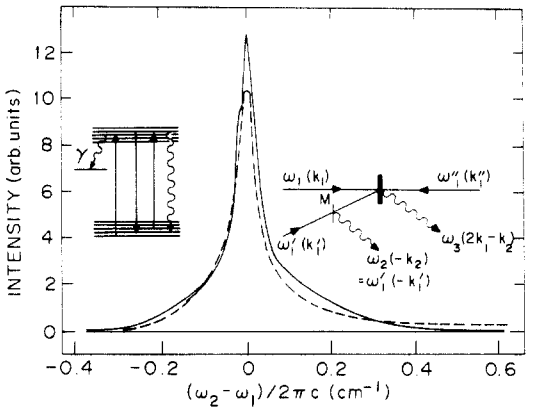

Figure 6. The diffracted light intensities around $\omega_1 - \omega_2 = 0$ in the phase conjugate configuration (solid curve) and the Rayleigh mixing configuration (dashed curve) for cresyl violet in ethanol. The specific beam configurations are shown as inserts. The widths are closely related to the population decay $1/\gamma$. After ref 21.

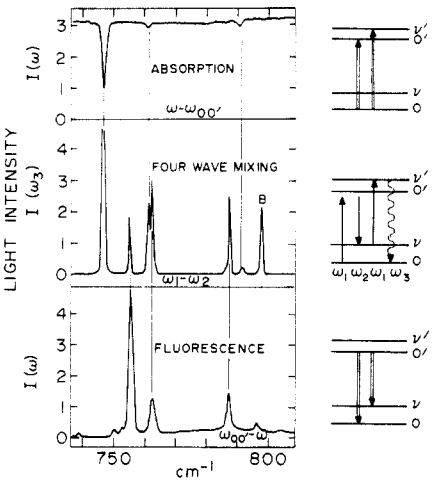

Figure 7. Absorption (upper), fluorescence (lower), and CARS four-wave mixing spectra (middle) of pentacene in a benzoic acid crystal at 1.6 K. The four-wave mixing spectrum was measured on a crystal of 5×10^{-7} mol/mol concentration and ω_1 was in exact resonance with the 0–0′ transition of pentacene. The band B is a benzoic acid CARS resonance and can be used for calibration of the signal since it has a conventional off-resonance Raman cross section comparable with the 992-cm^{-1} mode of benzene. After ref 26.

quantum statistical theory of the three-level system driven by two fields predicts sharp changes in the slope of the log I_3 vs. log $(\omega_1 - \omega_2)$ curve at $\omega_1 - \omega_2 \approx \Gamma$ and $\omega_1 - \omega_2 \approx \Gamma$, with steps (marked by a and b in Figure 5) in the curve when there is cross-relaxation or spectral diffusion occurring.

For Rh-6G in ethanol we found $T_2 = 0.05$ ps, which was about the same as the cross-relaxation time in the inhomogeneous distribution. One conclusion from this study was that the width of the linear absorption spectrum is influenced by spectral cross-relaxation in which the individual molecular transition frequencies spread across the whole absorption range on the time scale of 50 fs. This same result was not found for all the molecules studied. For example, for cresyl violet described by the same model, the cross-relaxation spread the frequencies over only about one-fifth of the absorption region.

With the experimental configuration shown in Figure 6 the three incident fields induce three different gratings in the sample. When all the frequencies are equal (degenerate four-wave mixing), these gratings are stationary in the medium. For example, the conjugate wave at $\omega_1'(-k_1')$ of Figure 6 results from the diffraction of ω_1'' and ω_1 from the gratings formed by the ω_1,ω_1' and ω_1'',ω_1' pairs, respectively. The beam labeled ω_3 originates from the diffraction of ω_1' from the grating formed by the ω_1,ω_1'' pair. Figure 6 shows spectra obtained for different beam configurations in the vicinity of $\Delta\omega = 0$. In this case the line shapes are directly related to the population decays of the levels that are driven by the fields. The population is caused to oscillate at the difference frequency $\omega_1 - \omega_2$ so that the effect of the populations on the response is present only in the range $|\omega_1 - \omega_2| \simeq \gamma_i, \gamma_j$.

Four-Level Systems

In order that a general four-wave mixing process be fully resonant the system must have four levels and each of these levels must be connected to two other levels by a one photon allowed transition (see Figure 1). This condition is very naturally met in molecules when the fundamental frequencies are in the range of electronic or vibronic transitions and when their differences equal vibrational or rotational frequencies. With only two different incident laser beams, just two resonance conditions can, in general, be fulfilled simultaneously, but in molecular systems a third resonance is also met approximately in as far as vibrational frequencies in different electronic states are similar. With use of three tunable input frequencies exact resonance can of course be achieved for all possible transitions. The susceptibility of a medium of noninteracting molecules is proportional to the number density, and the measured coherent signals are proportional to $|\chi|^2$. For a fully resonant four-level system, however, the susceptibility may become very large and not only allow the study of extremely dilute samples (ca. 10^{-2} ppm) but also make it possible to address and study specific molecular species in selected states and/or environments.

In our studies the dilute mixed crystal system pentacene dispersed in benzoic acid was used as a resonant nonlinear medium. The host, benzoic acid, forms high-quality crystals that are transparent not only to the visible frequencies ω_1 and ω_2 but also to $2\omega_1$ and $2\omega_2$. This system is expected to correspond closely to the theoretical model that treats two monochromatic waves at ω_1 and ω_2 coupled to a four-level system having resonances near ω_2, ω_1, $\omega_1 - \omega_2$, and $2\omega_1 - \omega_2$. The four levels correspond to the zeropoint levels (0 and 0′) of ground and excited states and any pair of vibrational levels v and u', one chosen from each of these states, for which $\mu_{vu'}$ is nonzero. The case where $v = u$, so that the same mode is involved in each state, was studied in detail.

Fully Resonant Coherent Raman Experiments

Our first fully resonant experiments used the CARS method with ω_1 fixed at the 0–0 transition and ω_2 tunable in the region of the fluorescence lines.[26] An intense

(22) T. Yajima, H. Souma, and Y. Ishida, *Opt. Commun.*, **18**, 150 (1976).
(23) J. R. Andrews and R. M. Hochstrasser, *Chem. Phys. Lett.*, **76**, 207 (1980).
(24) J. R. Andrews and R. M. Hochstrasser, *Chem. Phys. Lett.*, **76**, 213 (1980).

beam is generated in the direction $2\vec{k}_1 - \vec{k}_2$ having the anti-Stokes frequency $2\omega_1 - \omega_2$. The resonantly enhanced signals can be many times stronger than those from the host crystal notwithstanding the fact that the observed light intensity varies with the square of the concentration. For this case the enhancement factor was found to be greater than 10^{15}! The spectra shown in Figure 7 are typical. The four-wave mixing signal is seen to contain the information from both absorption and emission spectroscopy. Actually the resonant part of the homogeneous response in this case takes the form

$$\sum_{u,v} \frac{(1/\Gamma_{00'})\mu_{00'}\mu_{0'v}\mu_{vu'}\mu_{u'0}}{[i(\omega_{u'} - \Delta) - \Gamma_{u'0}][i(\omega_v - \Delta) - \Gamma_{v0}]} \quad (7)$$

where ω_v and $\omega_{u'}$ are ground- and excited-state vibrational frequencies corresponding to modes v and u and $\Delta = \omega_1 - \omega_2$. The signal is the square of this function with peaks at $\Delta = \omega_v$ and $\Delta = \omega_{u'}$ for all modes u and v for which transition moments in the numerator exist. For many molecules, however, the dominant contribution comes from $v = u$. This results from the fact that $\mu_{vu'}$ is often maximum when $\mu = v$, especially in large molecule spectra. In addition $\omega_v - \omega_{v'}$ is frequently smaller than $\omega_v - \omega_{u'}$ and the contribution of each term in the sum to the signal at the peaks is inversely proportional to $(\omega_v - \omega_{u'})^2$. Indeed, intense signals are obtained from modes that have nearly the same frequency in the ground and excited states since then both factors in the denominator of eq 7 become small at about the same value of Δ. An example, shown in the Figure 7, is the mode at $\omega_v = 762$, $\omega_{v'} = 761$ cm^{-1}, which shows only a weak absorption line but a relatively strong doublet in the coherent experiment. The presence of $\mu_{vu'}$ in eq 7 means the transition $u' \rightarrow v$ must be allowed for a signal to be observed. This implies that the states u' and v must be from the same symmetry species. Thus this technique can be used to identify the occurrence of different components in a mixture, different sites such as in mixed crystals, a Shpolski hydrocarbon matrix, and matrix isolated species or different aggregates of the same species.

In cases when the driving laser spectral bandwidth incorporates an ensemble of four-level systems having a distribution of transition frequencies, the resonance response (although not the actual lineshapes) is well-represented by an expression like eq 7 but with the Γ's interpreted as inhomogeneous line widths.[27] This would arise if the level shifts in the inhomogeneous distribution were proportional to the transition frequencies (as in the Doppler effect) or if there were no correlations between the distribution of spectral shifts for the different transitions within the four-level system. Some situations are predicted to yield lines that are narrower than the inhomogeneous widths, such as the case of the ensemble average of eq 8 with vibrational transitions having shifts opposite in sign to the electronic shifts. Another situation in which line narrowing can occur is with coherent Stokes generation, but in a four-level system such as discussed here this process is more complex than CARS and cannot be described by just a single term analogous to eq 7.

(25) E. J. Heilweil, R. M. Hochstrasser, and H. Souma, *Opt. Commun.*, **35**, 227 (1980).
(26) P. L. DeCola, J. R. Andrews, R. M. Hochstrasser, and H. P. Trommsdorff, *J. Chem. Phys.*, **73**, 4695 (1980).
(27) B. Dick and R. M. Hochstrasser, *J. Chem. Phys.*, **78**, 3398 (1983).

New Effects in Resonant Coherent Stokes Generation

There are three fully resonant time orderings that contribute to the generation of Stokes radiation in a four-level system.[28] These are inserted in Figures 8 and 9. The second diagram differs from the first in that the initial ω_1 field is interchanged in time with the ω_2 field. Both these processes involve introducing coherence into the level pair $v'0'$ (the excited-state Raman transition). The third diagram is obtained when ω_1 and ω_2 transfer coherence directly into the $v0$ level pair (the ground-state Raman transition). The third diagram represents a process that is readily distinguished from the others by time-separated pulse experiments. For example, the experiment of time-resolved CARS described above can be accomplished in Stokes, using this diagram with $\omega_2 - \omega_1 = \omega_v$. Generally, when coherence is introduced into a pair of levels by a sequence of driving fields, the response function will exhibit a resonance when the transition frequency (see Figure 1) matches the appropriate combination of applied frequencies. While each of the two first terms in Figure 8 resonate on $\omega_{v'} = \omega_2 - \omega_1$, it turns out that the sum of these terms need not display this resonance. In fact, this excited-state Raman resonance is predicted to be absent if the quantity $\Gamma = \Gamma_{00'} + \Gamma_{0v'} - \Gamma_{0'v}$ is exactly zero.[28,29] From the definition in eq 1 one sees that $\Gamma = 0$ when the pure dephasing (elastic) parts of the coherence decay vanish in a system where the initial state does not decay. The response as a function of $\Delta = \omega_2 - \omega_1$ is given approximately by

$$\left(\frac{1}{[(\omega_{v'} + d - \Delta) + i\Gamma_{0v'}]}\left\{\frac{1}{(\omega_v - \Delta) + i\Gamma_v} + \frac{i\Gamma}{[(\omega_{v'} - \Delta) + i\Gamma_{v'}][(\omega_v - d - \Delta) + i\Gamma_{0'v}]}\right\}\right) \quad (8)$$

The absolute square of this function yields resonances at $\omega_{v'} + d$ (see Figure 8) and $\omega_v - d$, both of which have electronic transition widths, and resonances at ω_v and $\omega_{v'}$ having the Raman widths of each of the two electronic states. This interesting prediction implies that in the condensed phase at near the absolute zero of temperature where the pure dephasing might be small, one may expect little or no resonant enhancement of the Stokes signal from the condition $\omega_2 - \omega_1 = \omega_{v'}$. On the other hand, at finite temperatures the excited state Raman process is predicted to appear. This effect is termed[29] dephasing induced coherent emission (DICE). From the standpoint of spectroscopy it has important consequences since inter-excited-state transitions can be studied without first populating the excited states. The populations are introduced by pure dephasing, or collisional redistribution in gases, in the same process that converts Raman scattering into fluorescence emission.[30] The predicted temperature effects bring forth a method to measure directly the pure dephasing of transitions. Other coherent techniques such as photon echoes and holeburning spectroscopy measure

(28) N. Bloembergen, H. Lotem, and R. T. Lynch, Jr., *Ind. J. Pure Appl. Chem.*, **16**, 151 (1978).
(29) J. R. Andrews and R. M. Hochstrasser, *Chem. Phys. Lett.*, **83**, 427 (1981).
(30) R. M. Hochstrasser and F. Novak, *Chem. Phys. Lett.*, **53**, 3 (1978); R. M. Hochstrasser and C. A. Nyi, *J. Chem. Phys.*, **70**, 1112 (1979); R. M. Hochstrasser, F. Novak, and C. Nyi, *Isr. J. Chem.*, **16**, 250 (1977).

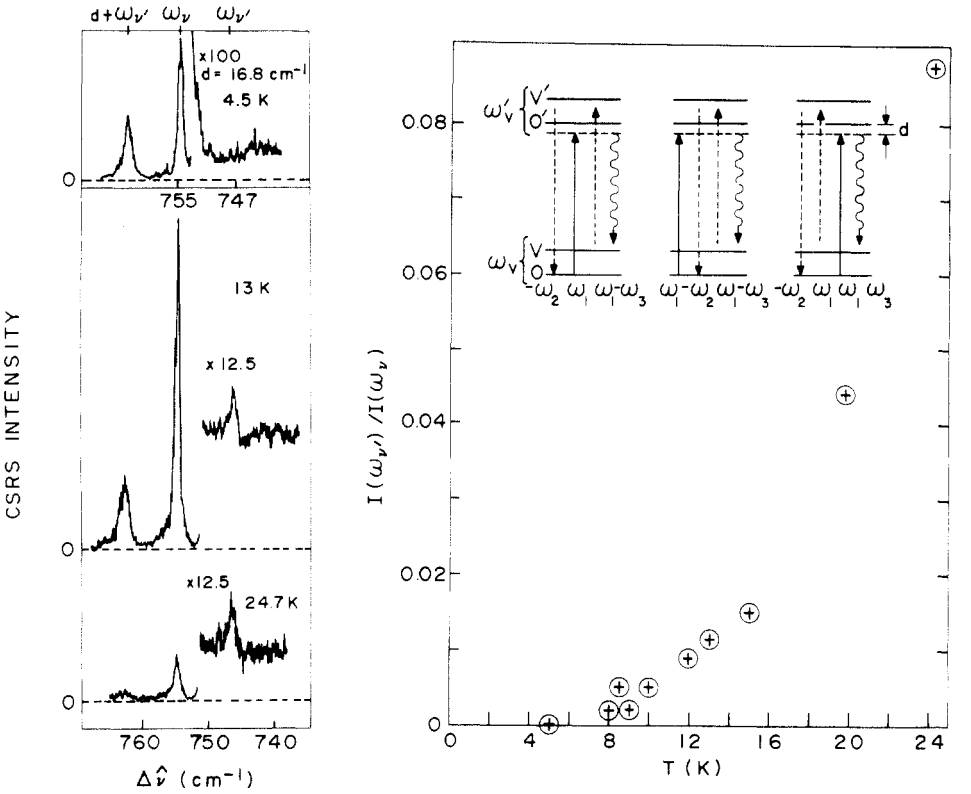

Figure 8. Coherent Stokes Raman spectra as a function of temperature of pentacene in a benzoic acid crystal. The frequency of ω_1 is set at 16.8 cm^{-1} lower than the 0–0′ transition of pentacene. At low temperature (4.5 K) resonances occur when $\omega_2 - \omega_1$ equals the ground-state vibrational frequency ω_v (755 cm^{-1}) and when the ω_2 beam matches the transition frequency of the vibronic transition $\omega_{00'} + \omega_{v'}$ (thus $\omega_2 - \omega_1 = \omega_{v'} + 16.8$ cm^{-1}). As the temperature is raised the growth of the excited-state vibrational resonance at $\omega_2 - \omega_1 = \omega_{v'}$ (747 cm^{-1}) is observed, while simultaneously the vibronic resonance loses its intensity. The ratio of the signal intensities at $\Delta = \omega_{v'}$ and $\Delta = \omega_v$ is plotted vs. temperature in the range 4.2–24 K. After ref 31.

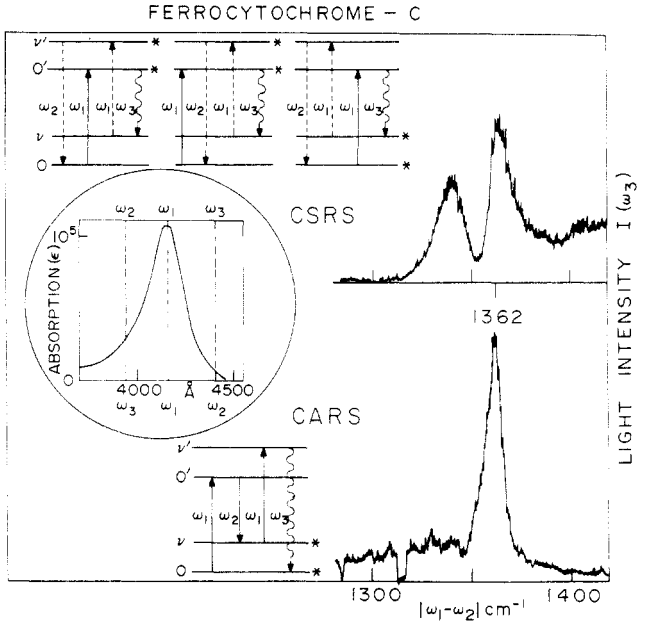

Figure 9. Four-wave mixing in a solution of ferrocytochrome *c* at room temperature. The location of the laser frequencies with respect to linear absorption spectrum are shown in the insert. In both the CARS and CSRS spectra ω_1 is at the peak of the Soret absorption band. The resonance at $|\omega_1 - \omega_2| = 1362$ cm^{-1}, which appears in both spectra, corresponds to a known ground-state vibration; the extra resonance, observed in the CRSRS spectrum at 1339.5 cm^{-1}, is perhaps the corresponding vibrational level in the Soret excited state. After ref 33.

only the total dephasing rate. The results for Stokes generation using pentacene in benzoic acid are given in Figure 8. The DICE effect growth of intensity at the resonance condition $\omega_2 - \omega_1 = \omega_{v'}$ compared with that at $\omega_2 - \omega_1 = \omega_v$ is apparent and is attributed to the onset of pure dephasing in the system.[31] DICE processes are, in fact, accounted for in the usual form of the resonant susceptibility[28,31] and were recently seen also in atomic vapors.[32]

More Complex Level Systems

It was natural to extend these nonlinear methods of obtaining excited-state Raman spectra to systems where no a priori knowledge about the vibrational structure in the excited state is obtainable by conventional spectroscopic techniques. Cytochrome *c* is a relatively simple protein and the visible and near-UV transitions of the Fe–porphyrin chromophore have been widely studied. The spontaneous Raman scattering, resonance enhanced by the intense Soret transition at 416 nm has been studied by numerous investigators. The prominent feature is the 1362-cm^{-1} mode known as an oxidation state marker band of the iron–porphyrin system. The Soret band is a single peak with a full width of ca. 1300 cm^{-1}, having no apparent underlying structure. Questions have frequently arisen as to the nature of the line width, whether it is dominated by population relaxation (lifetime broadening), pure dephasing, inhomogeneous effects, underlying congestion of levels, and so on.

We measured the dispersion of the Stokes and anti-Stokes generated light of ferro- and ferric-

(31) J. R. Andrews and R. M. Hochstrasser, *Chem. Phys. Lett.*, **82**, 381 (1981).
(32) Y. Prior, A. R. Bogdan, M. Dagenais, and N. Bloembergen, *Phys. Rev. Lett.*, **46**, 111 (1981).

ytochrome *c* at various concentrations and at different fixed frequencies of ω_1 scanning ω_2. A typical result is shown in Figure 9. As expected a single strong resonance at $\omega_1 - \omega_2 = 1362$ cm^{-1} is observed in the CARS spectra. The same resonance is recorded in the CSRS spectra, but in addition a new resonance appears at $\omega_2 - \omega_1 = 1339.5$ cm^{-1}. This result is expected for the level structure of Figure 9 if we assign the new resonance to the excited-state Raman transition $0' \rightarrow v'$. This resonance should show up in the CARS spectra if there are states near $2\omega_1$ connected to the ground state by a strong two photon allowed transition (see diagrams 1a and 1b in Figure 1). Indeed the best agreement with the experimental CARS spectra is obtained when small contributions of this type are included. With such contributions the CSRS spectra as well as their observed concentration dependence could be fitted quantitatively and all available experimental evidence is therefore consistent with the proposed assignment of these "extra resonances" as being a DICE effect.[33]

The line widths of our nonlinear spectra indicated that the lifetime of the Soret state is at least 0.7 ps. For ferricytochrome *c* our measurements indicated that the CSRS spectra also do contain a contribution from the corresponding excited-state vibrational mode. The lifetime of the Soret state required to fit the nonlinear response was approximately 0.3 ps.

The level structure and dynamics of systems such as cyctochrome *c* are terribly complex and much work remains to be done before it will be clear that models, such as the one indicated in Figure 9, can be used to describe the nonlinear response. Nevertheless additional insight is expected to arise from an improved understanding of nonlinear spectra of such systems, and these experiments with cytochrome *c* just scratch the surface of a whole new area of spectroscopy that still has major theoretical and experimental problems to explore. In the few examples given here it was seen that nonlinear optical processes are specific in space, time, species, and the quantum state of the system. Not only can they probe ultrafast processes but they are easily adapated to ultrahigh-resolution spectroscopy even in systems that are inhomogeneous. Future research will have to be concerned with sensible chemical approaches to the calculation of the nonlinear susceptibilities and with the effects of very strong light fields for which the perturbative attitudes of the present article are no longer appropriate.

(33) J. R. Andrews, R. M. Hochstrasser, and H. P. Trommsdorff, *Chem. Phys.*, **62**, 87 (1981).